Heliyon 10 (2024) e38929

Contents lists available at ScienceDirect

Heliyon

journal homepage: www.cell.com/heliyon

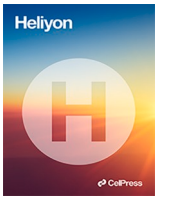

Research article

Biomechanical properties analysis of posterior lumbar interbody fusion with transpedicular oblique screw fixation

Li Wu [a,*], Xiaoxuan Jiang [a], Tianmin Guan [a], Zhong He [b], Jian Li [a,c]

[a] Institute of Mechanical Engineering, Dalian Jiaotong University, Dalian, 116028, Liaoning, China
[b] Nanjing Drum Tower Hospital, the Affiliated Hospital of Nanjing University Medical School, Nanjing, 210009, Jiangsu, China
[c] Orthopedics, Dalian University Affiliated Xinhua Hospital, Dalian, 116021, Liaoning, China

A B S T R A C T

Objective: An alternative to conventional posterior lumbar interbody fusion (PLIF) is a PLIF with transpedicular oblique screw fixation system. An assessment of new fixation system's viability and efficacy is conducted through a comparison of its biomechanical properties with those of conventional PLIF.

Method: A comprehensive finite element model (FEM) of the lumbar regions L1-L5 was developed and the surgical segment L3-L4 was chosen to comprise the surgical models of both traditional PLIF and new PLIF. In new PLIF model, an analysis was conducted on segmental range of motion (RoM), cage stress, inferior endplates stress, vertebral stress, and internal fixation stress. Three-dimensional printers are utilized to fabricate and assemble the fusion cage and vertebrae, and compression test machines are employed to execute physiological load and extreme load experiments on new PLIF, so as to verify the accuracy of the FEM analysis and the mode of fatigue exhibited by new PLIF.

Results: In new PLIF, the maximum stress on the inferior endplates under physiological loads was reduced in comparison to conventional PLIF. While the maximum stress on the cage, vertebral body, and screw increased, it remained within an acceptable range. The experimental data indicates that new fixation system can endure a vertical load exceeding 2800 N and an ultimate bending moment of 77 Nm.

Conclusion: The new PLIF exhibits a comparable RoM to its predecessor, simultaneously mitigating inferior endplate stress and accommodating physiological loads, which reduce the amount of surgical incision and fusion fixation instruments. Consequently, it emerges as a sanguine surgical approach to fuse the degenerative lumbar spine.

1. Introduction

Degenerative diseases affecting the lumbar intervertebral disc were observed to have an incidence rate ranging from 5 % to 10 % worldwide [1]. As a mature surgical procedure, posterior lumbar interbody fusion (PLIF) was frequently employed to treat these conditions [2]. Nevertheless, the PLIF procedure required extensive tissue dissection, removal of substantial bone structures, and implantation of the screws and the rods to adjacent vertebral bodies; these procedures posed a risk of surgical site infection and compromised the posterior column's stability [3]. Numerous novel internal fixation systems have surfaced recently with the intention of enhancing stability and minimizing trauma during PLIF surgery [4]. The cage-equipped spinous process stabilization device was positioned between adjacent lumbar vertebral bodies; the resulting wound was more compact and possessed superior dynamic properties; however, it exhibited inferior stability [5]. Additionally, anterior titanium plate fixation and zero-p fusion cage implantation improved the stability of cervical fusion procedures, but were incompatible with PLIF fusion procedures [6]. Postoperative complications such as endplate fractures and cage settlement may result from PLIF fusion surgery if the cage is merely implanted [7].

* Corresponding author. Dalian Jiaotong University, 794 Huanghe Road, Shahekou District, Dalian, Liaoning, 116028, China.
E-mail addresses: djtuwuli@163.com, wuli@djtu.edu.cn (L. Wu), 2507012458@qq.com (X. Jiang), djtugtm@163.com (T. Guan), hezhong_nju@126.com (Z. He), djtulj@163.com (J. Li).

https://doi.org/10.1016/j.heliyon.2024.e38929
Received 30 May 2024; Received in revised form 22 September 2024; Accepted 2 October 2024
Available online 4 October 2024

To mitigate these complications, pedicle screws and other internal fixation devices must be inserted into the human body in conjunction with the cage [8,9]. Therefore, is there a method that effectively maintains the segment's stability and minimizes damage during PLIF fusion surgery?

The screw trajectory of the oblique lumbar fixation in the lumbosacral spine was documented in the 1990s, and patients with spondylolisthesis underwent pedicular transvertebral screw fixation [10–13]. In their investigation, Wu et al. examined the viability of employing oblique lumbar interbody fixation to insert screws for L1/2, L2/3, and L3/4 lumbar fixation using 3D digital images [3]. Based on the outcomes of data analysis from the 3D images, they devised interbody cages in the shape of trapezoids. Three cadaveric specimens were subsequently subjected to percutaneous posterior oblique screw fixation with lateral interbody fusion [14]. In a

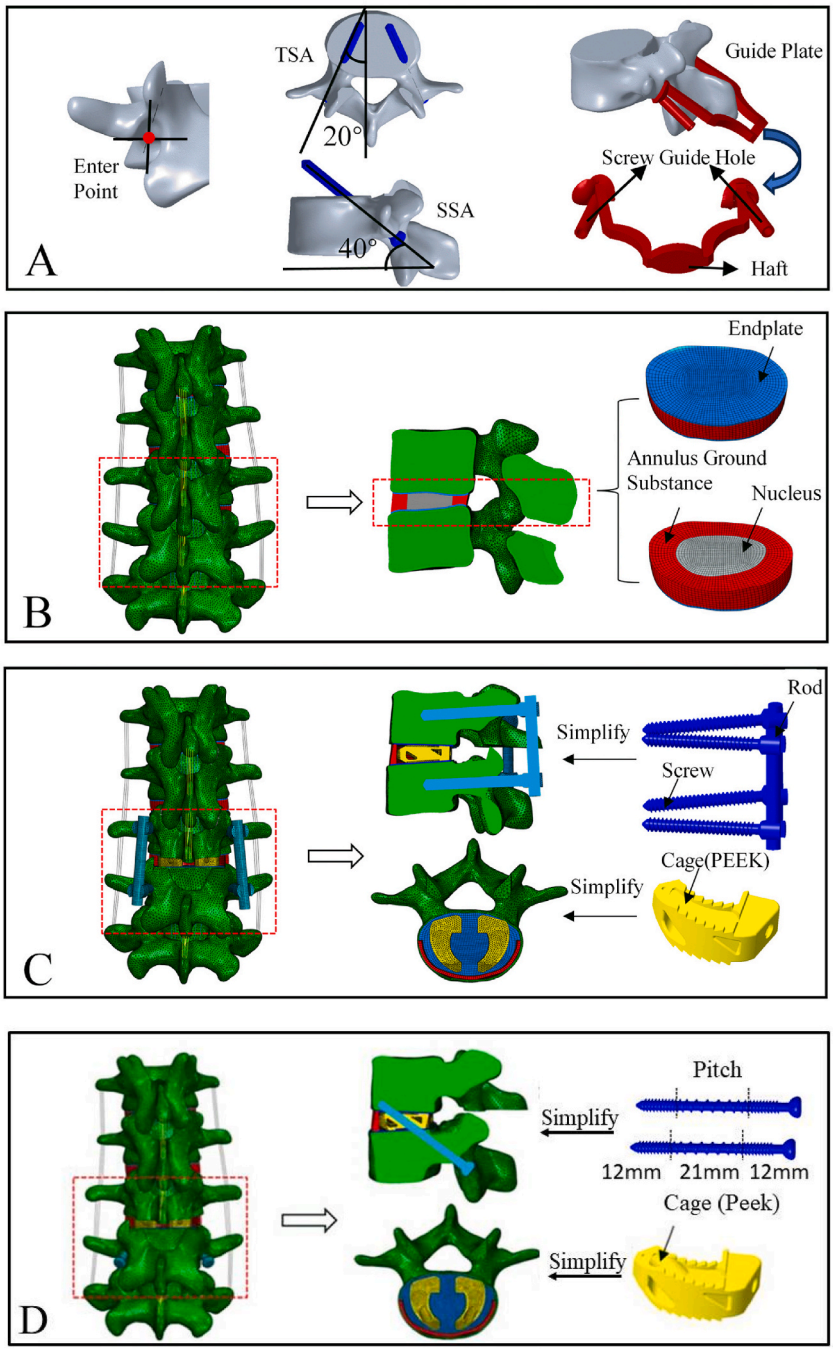

Fig. 1. Analysis model: Screw channel and guide plate for new internal fixation **A**); Construction of normal lumbar spine model **B**); Traditional PLIF model **C**); New PLIF model **D**).

human cadaveric model, Selvon et al. compared the range of motion (RoM) and fatigue mode following monosegmental oblique transpedicular and transdiscal fixation to conventional PLIF fixation [15]. The biomechanical properties of the novel transpedicular transdiscal (TPTD) screw fixation with interbody arthrodesis technique in the lumbar spine were examined by Qing et al. using finite element analysis [16]. Nevertheless, the model fails to include information regarding the precise design of the cage or the surgical operation plan. In order to find a fusion fixation method that is more in line with the biomechanical properties of the human body, a new fixation method of oblique upward screw insertion in the posterior lumbar pedicle is proposed in this paper, which can reduce the endplate subsidence phenomenon of the traditional screw-rod fixation system, and decrease the surgical trauma and the amount of fixation devices. A set of individualized design methods for fusion cages and screw fixation systems remains to be developed.

The paper presents a quantitative comparison of the spine segment RoM, as well as the mechanical properties of the cage, inferior endplate, and pedicle screw system, under six physiological loads, between the new and traditional PLIFs using the finite element method. A compression and bending experiment was performed on the assembled PLIF model, consisting of two 3D printed vertebral segments, two cages, and two screws. The results of the experiment were analyzed and compared in the paper.

2. Materials and methods

The posterior short segment internal fixation method (new PLIF) is a novel approach that utilizes a pair of pedicle screws. These screws enter the system through the pedicle channel on the inferior body, penetrate the inferior endplate, and then ascend diagonally through the cage channel to reach the superior endplate and cortical rim of the superior body (Fig. 1A). Determining the insertion position and direction of the screw is critical. To ascertain the accurate placement and trajectory of the screw, the personalized surgery guide plate is devised using data from the CT model, the CT scanning parameters refer to Ref. [17]. The entry point of the new fixation scheme was chosen from the entry point of the conventional cortical bone trajectory (CBT) during the design of the guide plate. Specific vertebral characteristics such as vertebral height, intervertebral height, and pedicle angle dictate the transverse screw angle (TSA) and sagittal screw angle (SSA) of the appropriate screw. Appropriate pedicle screws were chosen and positioned in accordance with the dimensions of the intended channel. These screws traversed the inferior body, traversed the cage predetermined on the basis of computed tomography (CT) data, and ascended to access the anterior vertebral body.

2.1. FEM of normal lumbar

After extracting the initial lumbar spine model from Mimics19.0 (Materialise Inc., Leuven, Belgium) using CT data from a healthy 30-year-old male volunteer, a comprehensive 3D geometric model of the lumbar spine L1-L5 was generated in Creo7.0 (Parametric Technology Corporation, Boston, Massachusetts, USA). Furthermore, the model for finite element analysis was established and defined in Abaqus 2020 (Simulia, Johnston, RI, USA) (Fig. 1B). The model comprises the following anatomical components: four pairs of articular cartilage; five vertebrae (each with upper and lower endplates, cancellous bone, and cortical bone); four intervertebral discs (comprising fibrous rings and nucleus pulposus); and seven sets of ligaments (including anterior longitudinal ligament, posterior longitudinal ligament, yellow ligament, transverse ligament, interspinous ligament, supraspinal ligament, and articular process ligament) [18]. Hypermesh14.0 is utilized for the fabrication of ligaments (Altair Engineering, Troy, Michigan, USA). Tables 1 and 2 [19–23] detail the element types and assigned finite element material parameters for each component.

2.2. FEM of the fixation system

The L3-L4 segment of a healthy lumbar spine is chosen for the implant cage in order to develop models of the fixation system. As illustrated in Fig. 1C and D, the FEM of the conventional PLIF, which comprised two titanium rods with a diameter of 6 mm and four pedicle screws measuring size Ø 6 * 50 mm, is established. Similarly, the FEM of the novel fixation system, which comprised two pedicle screws measuring size Ø 5 * 50 mm with changing pitch 1.75 mm and 3.5 mm, is also presented. The shape of the outer contour and the size and position of the Cage implanted in both models were the same to prevent unnecessary influence on the analysis results due to the change of Cage factors. The FEM model material parameters are detailed in Tables 1 and 2

In this case, the mutual contact parts between the screws, titanium rods, Cage and vertebral body models are set as bound contacts to simulate the stabilization of each part without slipping.

Table 1
FEM material properties of lumbar spine and implants.

Component	Element type	Young's modulus(MPa)	Poisson's ratio	Reference
Cortical bone	C3D4	12000	0.3	[19]
Cancellous bone	C3D4	100	0.2	[19]
Endplate	C3D8H	500	0.25	[22]
Annulus ground substance	C3D8H	4.2	0.45	[19]
Nucleus pulpous	C3D8H	Hyperelastic, Mooney–Rivlin C10 = 0.12, C01 = 0.03		[20]
Facet joint cartilage	C3D8H	24	0.4	[18]
Cage(PEEK)	C3D4	3600	0.25	[20]
Pedicle Screws	C3D4	110000	0.3	[19]
Titanium rods	C3D4	110000	0.3	[19]

Table 2
FEM parameters of lumbar ligaments.

Ligaments	Element type	Young's modulus (MPa)	Cross-sectional area(mm^2)	Reference
Anterior longitudinal	T3D2	7.8	63.7	[20]
Posterior longitudinal	T3D2	10	20	[18]
Ligamentum flavum	T3D2	15	40	[20]
Supraspinous	T3D2	8	30	[20]
Interspinous	T3D2	4.56	40	[20,21]
Intertransverse	T3D2	10	1.8	[20]
Capsular	T3D2	7.5	30	[20]

2.3. Experiment

Peek wire (Stratasys, 1.75 mm in diameter) and a high-temperature 3D printer (Stratasys Fortus 450mc, Eden Prairie, MN, USA) are utilized to fabricate the cage model. Using a high-temperature printer (Juying Y2020, Shenzhen, GuangDong, China) and peek

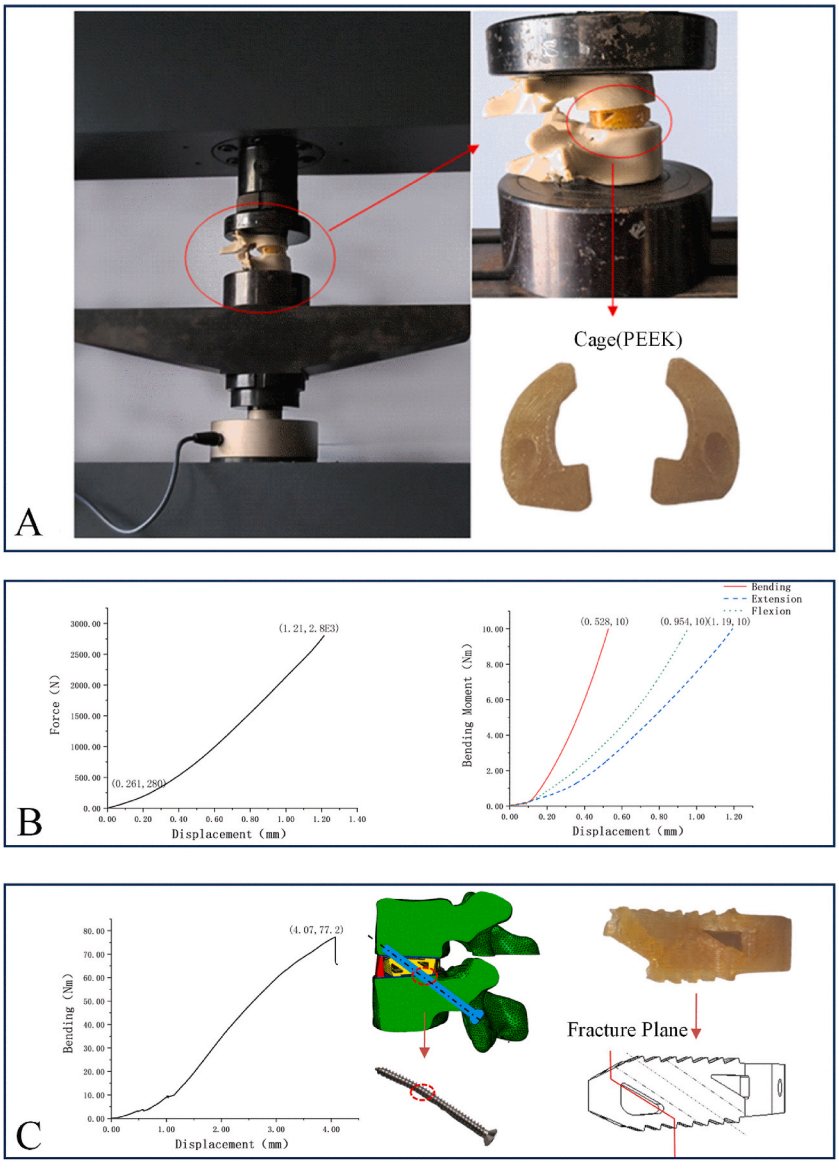

Fig. 2. Mechanical experiment and test results: Mechanical loading experimental machine and printed physical model **A**); Experimental results under compression and bending physiological load **B**); Ultimate load of flexion and failure state of new PLIF fixed system **C**).).

material (Yimai, Dongguan, GuangDong, China, 1.75 mm in diameter), the L3 and L4 vertebral bodies are printed. Since the modulus of elasticity of the peek material is closer to that of the vertebral cortical bone, the peek material was chosen for the printing of the vertebral body model in this study, and a lower print fill ratio was used to simulate the cancellous bone structure inside the vertebral body. As shown in Fig. 2 A, the assembled model is constructed in accordance with the new PLIF and placed on a mechanical testing machine (Suns UTM5150, Shenzhen, GuangDong, China) for compression and bending experiments.

The load was applied at a rate of 0.5 mm/min throughout the testing procedure, until it reached the predetermined physiological

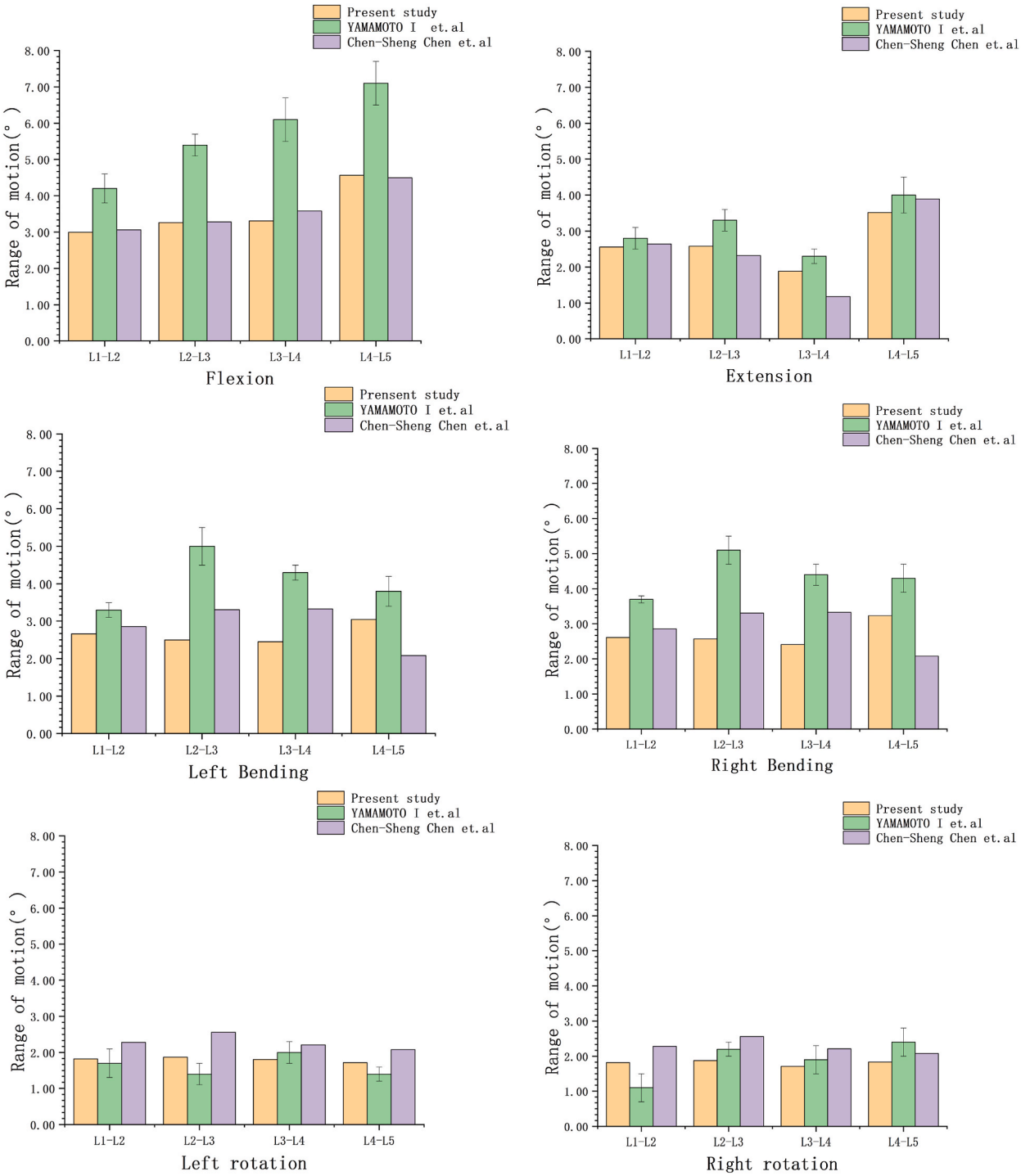

Fig. 3. Validation of lumbar L1-L5 range of motion (°).

load (compression load 280 N, bending load 10 Nm). At that point, the stress and displacement of the assembled model were recorded. Subsequently, the compression load is increased gradually to 2800 N, and the test model was not damaged. Finally, the bending load is incrementally augmented in the flexion condition until the model sustains damage.

3. Ethics approval and consent to participate

The present study was approved by the Ethics Committee of the Affiliated Xinhua Hospital of Dalian University. Informed consent obtained from the participant was written. All protocols are carried out in accordance with relevant guidelines and regulations.

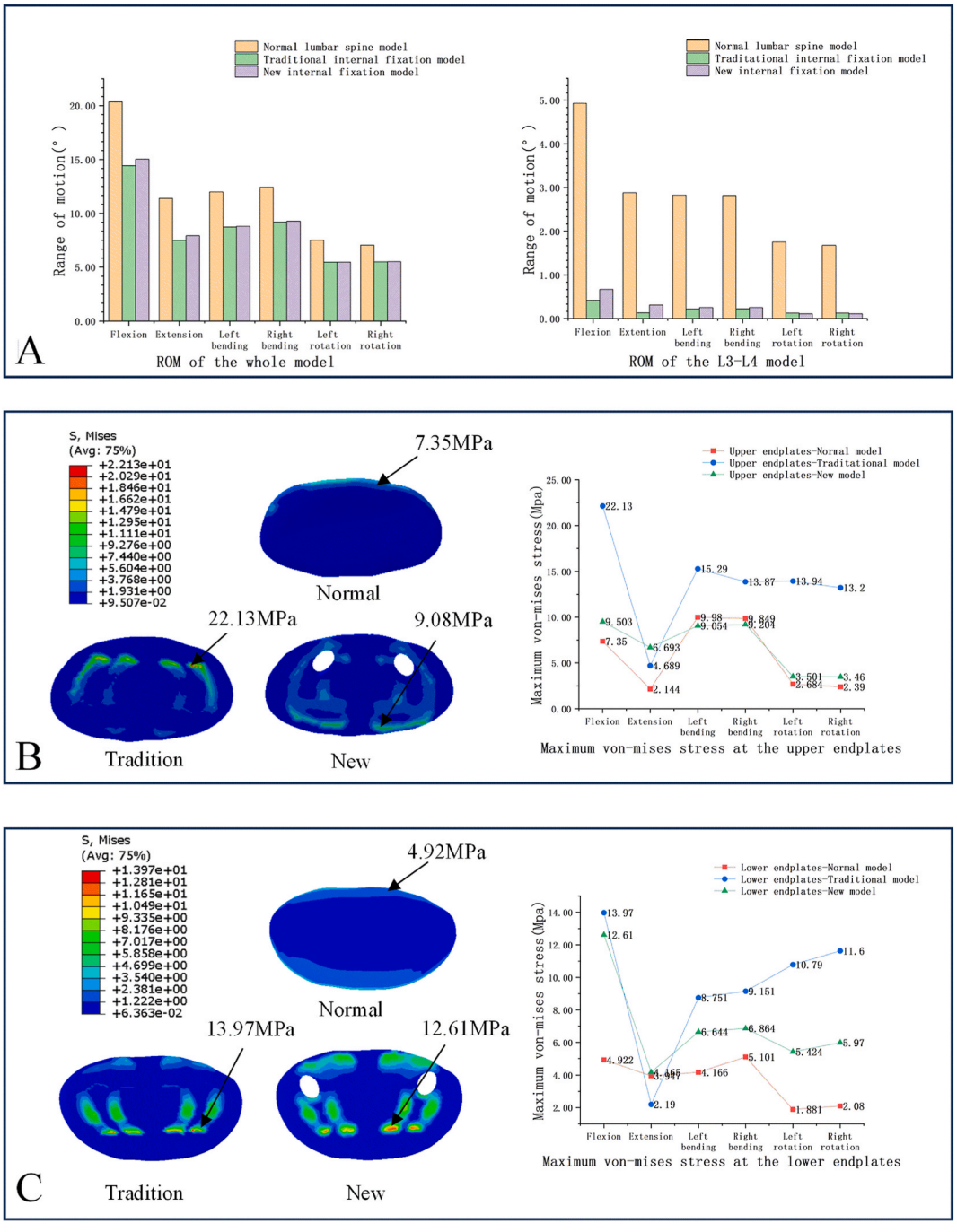

Fig. 4. Analysis results of 3 FEMs under six physiological conditions: RoM of overall lumbar and L3-L4 segment **A**); Upper endplate **B**); Lower endplate **C**); L3-L4 segment **D**), Cage **E**); Screw and rod **F**).

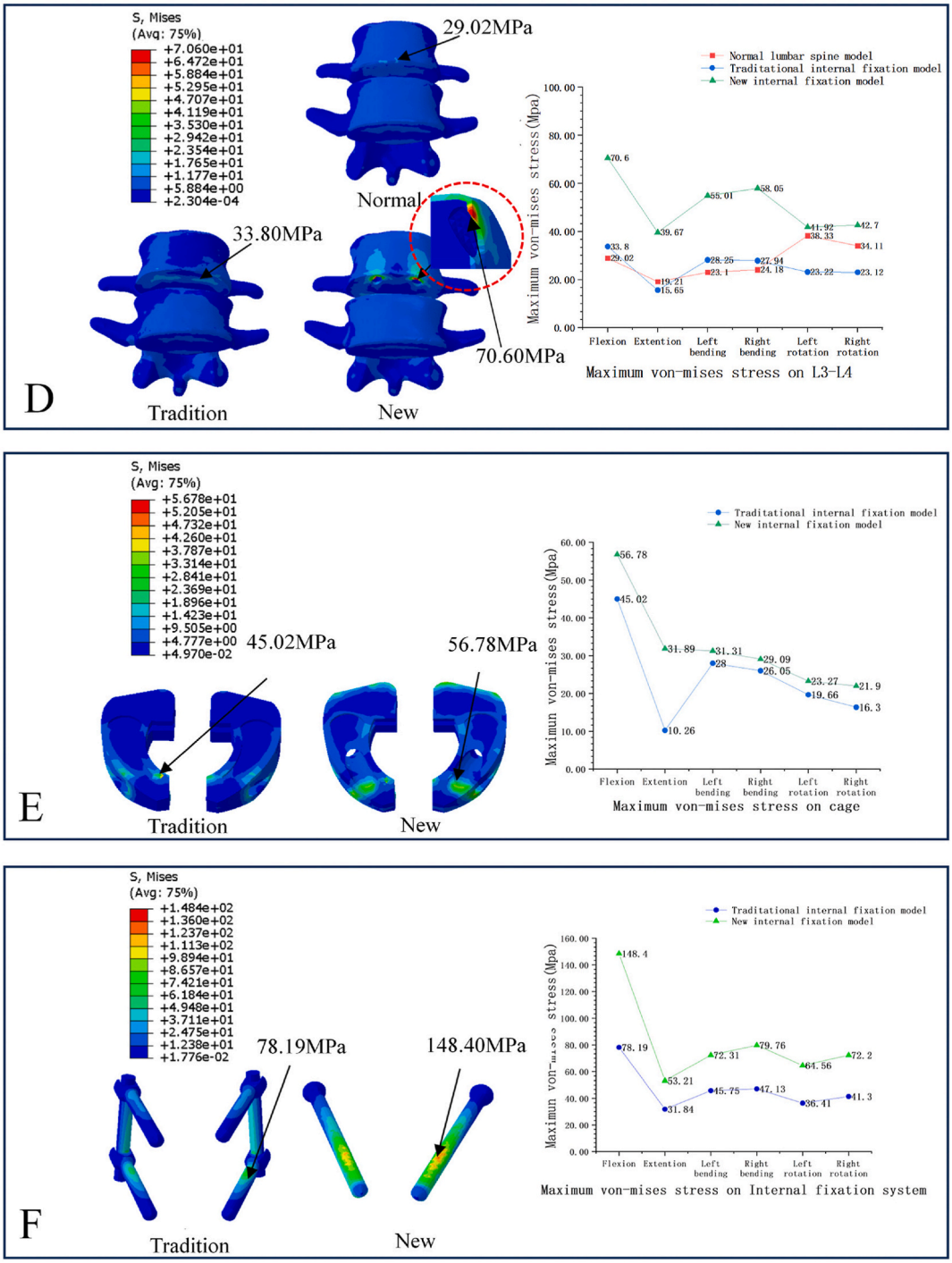

Fig. 4. (*continued*).

4. Result

4.1. Model validation

In order to simulate the axial load (i.e., upright position) of physiological compression, a vertical load of 150 N was applied to the upper surface of L1, in accordance with the normal lumbar spine model (Fig. 1 B). In addition, six distinct physiological movements of the lumbar spine were simulated using a bending moment of 10 Nm: flexion, extension, left bending (LB), right bending (RB), left

rotation (LR), and right rotation (RR). The surgical segment range of motion (RoM) was computed numerically and subsequently compared to the outcomes of prior in vitro investigations and finite element analysis (illustrated in Fig. 3) [24,25].

The agreement between the surgical segment RoM of the Lumbar Spine L1-L5 model and that documented in the literature (Fig. 3) confirms the normal lumbar spine model's validity.

4.2. Fixation system RoM

In accordance with the normal model (Fig. 1 B), the conventional PLIF model (Fig. 1C) and the new PLIF model (Fig. 1 D), the upper surface of L1 was subjected to a vertical load of 280 N to replicate the axial load of compression in its upright position, reflecting physiological conditions. Additionally, six distinct physiological movements of the lumbar spine were simulated by imposing a bending moment of 10 Nm [20,26].

As illustrated in Fig. 4A, the overall lumbar range of motion (RoM) for both fixation methods was considerably diminished during the six physiological movements compared to the normal model. Furthermore, the RoM of the L3-L4 segment was severely constrained by the fusion mechanism. In comparison to the conventional fixed model, the new fixed model exhibited an overall increase in activity of 4.25 %, 5.66 %, 0.65 %, 0.68 %, −0.03 %, and 0.24 % during the six physiological movements. Furthermore, the activity of the L3-L4 segments demonstrated respective increases of 60.53 %, 136.36 %, 16.51 %, 12.44 %, −14.17 %, and −14.17 %.

4.3. End plate stress

Maximum von Mises stresses on the upper and lower endplates of the normal model, the traditional fixed model, and the new fixed model were displayed in Fig. 4B and C, respectively, under the six physiological conditions. The maximum von Mises stress on the upper and lower endplates along the L3-L4 segment was considerably greater in the traditional fixed model compared to both the normal model and the new fixed model, it was discovered.

When comparing the new fixation model to the normal model, the stress on the upper endplate of the L3-L4 segment decreased marginally under the left and right lateral bending conditions, by 9.28 % and 6.55 %, respectively. Furthermore, the maximum stress value exhibited a progressive rise of 44.82 %, 29.29 %, 212.2 %, and 30.44 % under the remaining four conditions, respectively. Under six physiological movements, the stress on the lower endplate increased by a respective 156.2 %, 5.52 %, 59.48 %, 31.03 %, 188.4 %, and 186.5 %.

In contrast to the conventional fixed model, the new fixed model exhibited a reduction of 57.06 % in maximum von Mises stress at the upper endplate during forward bending, an increase of 42.74 % during backward stretching, and decreases of 40.78 %, 33.64 %, 74.89 %, and 73.77 %, respectively, during left and right lateral bending and lateral rotation. The stress on the lower endplate exhibited a 9.74 % decrease in the forward bending condition, a 90.18 % increase in the backward stretching condition, and reductions of 24.08 %, 24.99 %, 49.73 %, and 48.59 % in the left bending, right bending, left rotation, and right rotation conditions, respectively.

4.4. Vertebrae and cage stress

As shown in Fig. 4 D, the utilization of the new fixed model results in a notable increase in the maximum von Mises stress for the fusion segment of six physiological movements compared to the normal model. Specifically, the increase is as follows: 143.28 %, 106.51 %, 138.14 %, 140.07 %, 9.37 %, and 25.18 %, respectively. It exhibited respective increases of 108.88 %, 153.48 %, 94.73 %, 107.77 %, 80.53 %, and 84.69 % when compared to the conventional fixed model. Nevertheless, the von Mises stress peak during the six physiological movements was considerably diminished in comparison to the 110 MPa stress experienced by the lumbar vertebrae [22].

As shown in Fig. 4 E, the maximum stress of the cage in the new fixed model increases by 210.82 % during backward extension compared to the traditional fixed model. However, the stress increases by only 26.12 %, 11.82 %, 11.67 %, 18.36 %, and 34.33 % during the remaining five physiological movements, respectively, which were all significantly lower than the tensile strength of PEEK material (120 MPa) [27].

4.5. Fixture stress

As shown in Fig. 4 F, the maximum von Mises stress of the fixed device in the new fixed model increased noticeably during the six physiological movements, by 89.79 %, 67.12 %, 58.05 %, 69.23 %, 77.31 %, and 74.72 %, respectively, in comparison to the traditional fixed model. However, this increase was significantly less than the strength of the titanium alloy material in the pedicle screw system (862 MPa) [28].

4.6. Dynamic response

With the boundary constraint conditions of the model shown in Fig,1C and Fig. 1D, on the upper surface of L1 vertebral body, 400 N axial compressive force is applied to simulate the weight of the upper body of the human body, and at the same time, a sinusoidal axial load with an amplitude of 40 N and a frequency of 5 Hz is applied to simulate the vibration environment in which the human body is located. The dynamic stress and dynamic displacement of the new fixed model and the traditional fixed model under the repeated changing external force conditions are analyzed. As shown in Fig. 5, the dynamic stress and dynamic displacement of the new fixed

model and the traditional fixed model are both sinusoidal waves. The mean dynamic stress of the new fixed model is 14.8 MPa, and the amplitude is about 0.6 MPa; the mean dynamic stress of the traditional model is 11.7 MPa, and the amplitude is about 0.46 MPa. The mean dynamic displacement of the new fixed model is 0.36 mm, and the amplitude is 0.05 mm; the mean dynamic displacement of the traditional fixed model is 0.33 mm, and the amplitude is about 0.05 mm.

4.7. Experiment results

As illustrated in Fig. 2B and C, the displacement of the model during the compression experiment was recorded as 0.26147 mm when the load reached 280 N. Similarly, when the bending moment reached 10 Nm, the model experienced the following displacements: maximum flexion displacement of 0.9578 mm, maximum extension displacement of 1.19266 mm, and maximum left bending displacement of 0.52802 mm. The corresponding finite element analysis results for these displacements were 1.911 mm, 1.063 mm, and 0.591 mm, respectively, which indicate the feasibility of the FEM. The assembled fixation model is subjected to a vertical load of 2800 N without sustaining any damage; this demonstrated that the newly developed fixation system is capable of withstanding such a load. When the bending moment increased to 77 Nm, under the flexion condition, the cage ruptured at its front bone window, and a significant portion of the screw exhibited bending at one-third of its end. The experimental fracture position of the cage and bending position of the screw corresponded to the maximum stress positions predicted by the finite element analysis (Figs. 2C and Fig. 4 E, F, respectively).

5. Discussion

The RoM of the new fixation system during the six physiological movements of the L3-L4 segment was 0.671°, 0.312°, 0.254°, 0.253°, 0.109°, and 0.109°, all of which were within 1 % (Fig. 4A). This suggests that the postoperative fixation effect can be satisfactorily achieved using the proposed model [29]. The new fixation system exhibited an overall RoM of 15.023°, 7.913°, 8.789°, 9.265°, 5.467°, and 5.504°. Furthermore, under six physiological movements, the maximum error of the new fixation system's overall RoM is reduced to 5.66 %, a value that is in contrast to the conventional fixation method. This indicates that the new fixation system was capable of attaining a similar range of motion for the lumbar spine.

With regard to the end plate stress of the fusion segment, the maximum Von Mises stress on the end plate of the conventional fixed model was 22.13 MPa, 4.698 MPa, 15.29 MPa, 13.87 MPa, 13.94 MPa, and 13.22 MPa under the flexion, the extension, left bending (LB), right bending (RB), left rotation (LR), and right rotation (RR) conditions, respectively. In contrast, the end plate of the new fixed model experienced these stresses at values of 12.61 MPa, 6.693 MPa, 9.054 MPa, 9.204 MPa, 5.424 MPa, and 5.979 MPa. The comprehensive stress of the endplate of the new fixed model is lower than that of the conventional fixed model. Based on the findings reported in references [30] and [31], the endplate stress may serve as an indicator of the challenge associated with cage sinking. It demonstrated that the risk of endplate fracture was lower with the new fixation model compared to the conventional PLIF.

The new internal fixation system substantially elevated the maximum von Mises stress on the vertebrae, cage, and screw in comparison to conventional fixation systems. The reduction in force on the inferior endplate can be attributed to the force being transmitted through the screw, the cage, and the vertebral bodies via the screw connection between the two vertebral bodies and the cage in the new fixation system. The flexure condition resulted in the greatest stress on the vertebrae, screws, and cage, as illustrated in Fig. 4. This physiological movement may have posed a risk to the new fixation system. The region of the cortical bone where the screw head was affixed to the vertebral body experienced the highest stress on the vertebrae (70.60 MPa). This value was significantly lower than the maximum stress permissible on the vertebrae (110 MPa). The cage experienced a maximum stress of 56.78 MPa, which was

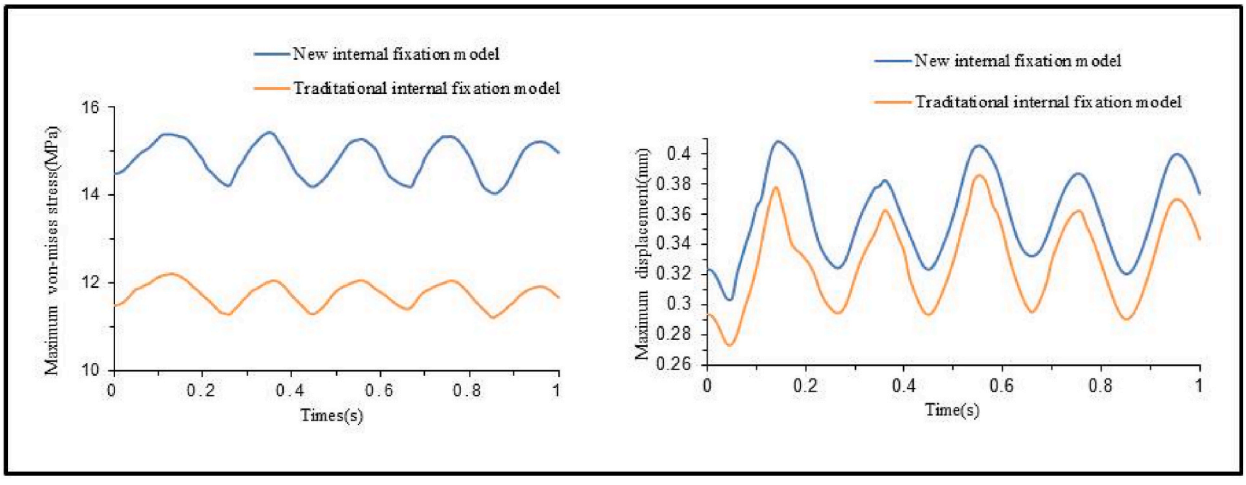

Fig. 5. Dynamic response of new fixation model and traditional fixation model.

significantly below the peak material's yield limit of 120 MPa. Additionally, the screw experienced a maximum stress of 148.4 MPa, which was significantly below the titanium alloy yield limit of 862 MPa. It demonstrated that the fracture failure of the screw and the cage would not be induced.

Under the condition of vibration load, the maximum dynamic stress and the maximum displacement of the new internal fixation model are slightly higher than those of the traditional internal fixation model, and the mean value and amplitude of its dynamic response are within the human body's bearing capacity range. It indicates that the new internal fixation model can also maintain stable displacement and internal stress under the condition of the dynamic changing load that the human body can bear, and there will be no shedding.

It is important to mention, however, that the analysis outcomes presented in the paper were calculated using an axial load of 280 N and a bending moment of 10 Nm in the direction of six distinct physiological movements. The centra experienced comparatively high levels of stress (70.6 MPa) when subjected to the flexure condition. Consequently, after surgery, forward bending movements under heavy load (28 kg) should be avoided if the new fixation scheme is implemented, otherwise, the fixed upper vertebral body is at risk of fracture.

The model remains in a normal state during compression experiments in which a vertical physiological load of 280 N is applied. Despite the subsequent increase in load to 2800 N, the newly installed fixed system has yet to sustain any damage. The model remains in a normal state during the flexion experiments when a flexion moment of 10 Nm is applied. The cage fractured at the front bone window when the moment was subsequently increased to 77 Nm under the flexion condition; this demonstrated that the newly developed fixation system could withstand the entire load range of typical physiological activities and meet the strength requirements. The study primarily examines the viability of implementing the novel fixation scheme. The subsequent phase entails the optimization of the fusion device's structure. The number of screws and rods is reduced in the new fixation system, which employs two pedicle screws for internal fixation as opposed to the conventional PLIF.

The above discussion show that the stress results of the new fixation method are comparable to the traditional fixation and the new fixation model can withstand the normal physiological load of the human body. Furthermore the fixation method use only two screw to immobilize the cage and the upper and lower vertebrae, so the surgical incision is small, and the amount of the fixation devices utilized is relatively small. So the new lumbar fusion fixation is worthy of promotion and application.

6. Conclusion

A novel PLIF fixation system is described in this article. In contrast to conventional PLIF, the lumbar range of motion (RoM) of the new PLIF is more analogous to that of a typical human model. The fact that the stress on the cage, vertebral body, and screw of the new fusion system is significantly lower than the allowable loads for PEEK, titanium, and compact bone, respectively, demonstrates that the new PLIF is safe. Bone fusion is facilitated and endplate sinking is averted by the increased cage stress and decreased inferior endplate stress. A promising posterior stabilization surgery strategy, it can decrease the surgical trauma area and the number of fixation devices utilized.

Data availability

The datasets used and/or analyzed during the current study are available from the corresponding author on reasonable request.

Funding

This study was funded by the Liaoning Natural Science Foundation of China (LJKMZ20220841, LJKZZ20220058).

CRediT authorship contribution statement

Li Wu: Writing – review & editing, Supervision, Funding acquisition, Conceptualization. **Xiaoxuan Jiang:** Writing – original draft, Software, Formal analysis. **Tianmin Guan:** Supervision, Conceptualization. **Zhong He:** Methodology, Conceptualization. **Jian Li:** Writing – review & editing, Data curation.

Declaration of competing interest

The authors declare that they have no known competing financial interests or personal relationships that could have appeared to influence the work reported in this paper.

References

[1] N.E. Epstein, A review of complication rates for anterior cervical diskectomy and fusion (ACDF), Surg. Neurol. Int. 10 (100) (2019) 1–8.
[2] J. Rathbone, et al., A systematic review of anterior lumbar interbody fusion (ALIF) versus posterior lumbar interbody fusion (PLIF), transforaminal lumbar interbody fusion (TLIF), posterolateral lumbar fusion (PLF), Eur. Spine J. 32 (6) (2023) 1–16.
[3] A.M. Wu, et al., A radiological and cadaveric study of oblique lumbar interbody fixation in patients with normal spinal anatomy, Bone Joint Lett. J. 95-B (7) (2013) 977–982.

[4] K.B. Fan, et al., Biomechanical analysis of double-level oblique lumbar fusion with different types of fixation: a finite element-based study, Orthop. Surg. 15 (2023) 1357–1365.
[5] W. Fan, et al., Biomechanical evaluation of rigid interspinous process fixation combined with lumbar interbody fusion using hybrid testing protocol, J. Biomech. Eng. 145 (6) (2023) 064501.
[6] P.R. Ouyang, et al., Computational comparison of anterior lumbar interbody fusion and oblique lumbar interbody fusion with various supplementary fixation systems: a finite element analysis, J. Orthop. Surg. Res. 18 (1) (2023) 1–13.
[7] G.F. Fang, et al., Biomechanical comparison of stand-alone and bilateral pedicle screw fixation for oblique lumbar interbody fusion surgery—a finite element analysis, World. Neurosurg. 141 (2020) e204–e212.
[8] Q.D. Wang, et al., Prediction of complications and fusion outcomes of fused lumbar spine with or without fixation system under whole-body vibration, Med. Biol. Eng. Comput. 59 (6) (2021) 1223–1233.
[9] Z.J. Zhang, et al., Biomechanical evaluation of four surgical scenarios of lumbar fusion with hyperlordotic interbody cage: a finite element study, Bio Med. Mater. Eng. 29 (4) (2018) 485–497.
[10] W.A. Abdu, et al., Pedicular transvertebral screw fixation of the lumbosacral spine in spondylolisthesis. A new technique for stabilization, Spine 19 (1994) 710–715.
[11] D. Grob, et al., Direct pediculo-body fixation in cases of spondylolisthesis with advanced intervertebral disc degeneration, Eur. Spine J. 5 (1996) 281–285.
[12] A. Minamide, et al., Transdiscal L5-S1 screws for the fixation of isthmic spondylolisthesis: a biomechanical evaluation, J. Spinal Disord. Tech. 16 (2) (2003) 144–149.
[13] C. Birkenmaier, et al., The European multicenter trial on the safety and efficacy of guided oblique lumbar interbody fusion (GO-LIF), BMC. Musculoskel. Dis. 11 (1) (2010) 199.
[14] A.M. Wu, et al., Percutaneous posterior transdiscal oblique screw fixation with lateral interbody fusion: a radiological and cadaveric study, Eur. Spine J. 24 (4) (2015) 852–858.
[15] C.S. Selvon, et al., Oblique lumbar interbody fixation: a biomechanical study in human spines, J. Spinal Disord. Tech. 25 (4) (2012) 183–189.
[16] Q.B. Lv, et al., Biomechanical properties of novel transpedicular transdiscal screw fixation with interbody arthrodesis technique in lumbar spine: a finite element study, J. Orthop. Transl. 15 (2018) 50–58.
[17] X. Datao, et al., Contribution of ankle motion pattern during landing to reduce the knee-related injury risk, Comput. Biol. Med. 180 (2024) 108965.
[18] H. Schmidt, et al., Intradiscal pressure, shear strain, and fiber strain in the intervertebral disc under combined loading, Spine 32 (7) (2007) 748–755.
[19] K. Alafate, et al., Hybrid pedicle screw and modified cortical bone trajectory technique in transforaminal lumbar interbody fusion at L4-L5 segment: finite element analysis, BMC. Musculoskelet. Disord. 24 (1) (2023) 288.
[20] S.F. Huang, et al., Biomechanical evaluation of an osteoporotic anatomical 3D printed posterior lumbar interbody fusion cage with internal lattice design based on weighted topology optimization, Int. J. Bioprint. 9 (3) (2023) 410–421.
[21] W. Fan, et al., Biomechanical analysis of lumbar interbody fusion supplemented with various posterior stabilization systems, Eur. Spine J. 30 (8) (2021) 2342–2350.
[22] M. El-Rich, et al., Finite element investigation of the loading rate effect on the spinal load-sharing changes under impact conditions, J. Biomech. 42 (9) (2009) 1252–1262.
[23] Z. Li Kh, et al., Establishment of finite element model of lumbar motion segments and its biomechanical significance, Chinese Journal of Tissue Engineering Research 9 (14) (2005).
[24] C.S. Chen, et al., Stress analysis of the disc adjacent to interbody fusion in lumbar spine, Med. Eng. Phys. 23 (7) (2001) 485–493.
[25] I. Yamamoto, et al., Three-dimensional movements of the whole lumbar spine and lumbosacral joint, Spine 14 (11) (1989) 1256–1260.
[26] Y.F. Yu, et al., Population-based design and 3D finite element analysis of transforaminal thoracic interbody fusion cages, J. Orthop. Transl. 21 (2020) 35–40.
[27] P. Sikder, et al., A comprehensive analysis on the processing structure property relationships of FDM-based 3-D printed polyetheretherketone (PEEK) structures, Materialia 22 (2022) 101427.
[28] A. Sharma, et al., Experimental study of machining characteristics of titanium alloy (Ti–6Al–4V), Arab. J. Sci. Eng. 38 (2013) 3201–3209.
[29] H.N. Boustani, et al., Which postures are most suitable in assessing spinal fusion using radiostereometric analysis? Clin. Biomech. 27 (2) (2012) 111–116.
[30] M. Zhang, et al., Long-term effects of placing one or two cages in instrumented posterior lumbar interbody fusion, Inter. Orthop. 40 (2016) 1239–1246.
[31] H. Xu, et al., Biomechanical comparison of transforaminal lumbar interbody fusion with 1 or 2 cages by finite-element analysis, Oper. Neurosurg. 73 (2) (2013) ons198–ons205.